CLOSED-LOOP AEROMECHANICAL STABILITY ANALYSIS OF HHC AND IBC, WITH APPLICATION TO A HINGELESS ROTOR HELICOPTER

Marco Lovera*, Patrizio Colaneri†
Dipartimento di Elettronica e Informazione, Politecnico di Milano
Piazza Leonardo da Vinci 32, 20133 Milano, Italy

Carlos Malpica‡, Roberto Celi§
Dept. of Aerospace Engineering, University of Maryland
College Park, MD 20740

Abstract

The paper summarizes a simple state space derivation for the continuous time form of the SISO HHC compensator; demonstrates how the same approach can be used to work out a state space representation for a SISO periodic HHC compensator, suitable for stability and robustness analysis; generalizes that result to get to a general approach for the derivation of the state space form for a MIMO HHC controller; and presents the results of a numerical investigation into the performance and stability properties of Higher Harmonic Control, implemented in the rotating system, based on a simulation study of the coupled rotor-fuselage dynamics of a four bladed hingeless rotor helicopter.

The results show that the IBC controller is very effective in reducing the 4/rev CG accelerations. The percentage reductions obtained in the simulations are in excess of 80-90%. The vibration attenuation occurs within 5-7 seconds after the IBC system is turned on. This is equivalent to a frequency of around 1 rad/sec, which is a frequency at which flight control systems and human pilots can operate. Therefore, the interactions and potential adverse effects on the stability and control characteristics of the helicopter should be explored. The IBC problem is intrinsically time-periodic if the IBC inputs include frequencies other than the frequency one wishes to attenuate. This is true even if the rest of the model is assumed to be time-invariant. In these cases, the closed-loop stability results obtained using a constant coefficient approximations may be incorrect even at lower values of the advance ratio μ, where constant coefficient approximation of the open-loop dynamics are accurate.

Notation

$A(t)$	Open loop stability matrix
A_0	Stability matrix (constant approximation)
B	Number of blocks in the Harmonic Transfer Function
$B(t)$	Input (control) matrix
$C(t)$	Output (measurement) matrix
C_T	Rotor thrust coefficient
$D(t)$	Direct Input/Output matrix
K	Gain of HHC controller
m	No. of control inputs
N	Number of rotor blades
n	No. of measured outputs
n_s	System order
p	No. of measured outputs
T	Rotor revolution period
t	Time
u	Input vector
y	Output vector
ψ	Azimuth angle of reference blade, $\psi = \Omega t$
Ω	Rotor angular velocity
Abbreviations	
CG	Center of mass of the helicopter
HHC	Higher Harmonic Control
HTF	Harmonic Transfer Function
IBC	Individual Blade Control
LTI	Linear Time Invariant (or constant-coefficient) model
LTP	Linear Time Periodic (or periodic-coefficient) model
MIMO	Multi-Input Multi-Output system
PHHC	Periodic Higher Harmonic Control
SISO	Single-Input Single-Output system

Introduction

Higher Harmonic Control (HHC) and Individual Blade Control (IBC) have been considered for many years as a viable approach for the design and the implementation of active rotor control laws aiming at the attenuation of helicopter vibrations (see, e.g., the recent survey papers [1, 2]). The main idea of HHC and IBC is to try and at-

*Associate Professor, lovera@elet.polimi.it
†Professor, colaneri@elet.polimi.it
‡Graduate Res. Assistant, cmalpica@eng.umd.edu
§Professor, celi@eng.umd.edu
Presented at the 29th European Rotorcraft Forum, Friedrichshafen, Germany, September 16-18, 2003.

tenuate N/rev vibratory components in the fuselage accelerations (N being the number of rotor blades) or in the rotor hub loads by adding suitably phased N/rev components to the rotor controls, either in the fixed (HHC) or rotating (IBC) frame. A number of studies have been carried out in order to determine the feasibility of active vibration control both from the theoretical and the experimental point of view; in particular, as far as the analysis of the dynamic behaviour of the single-input single-output (SISO) HHC is concerned, a fundamental result was given in [3] where a continuous time analysis of HHC was carried out for the first time and it was shown that to first approximation the classical T-matrix HHC algorithm (see [4]) can be written as a linear time invariant dynamic compensator. More recently, however, it has been proposed to try and exploit the *interharmonic coupling* due to the periodicity of rotor dynamics in forward flight ([5]) in order to achieve the attenuation of N/rev vibrations by means of lower frequency inputs, such as, e.g., 2/rev or 3/rev for a 4 bladed rotor. To this purpose, a generalization of the T-matrix algorithm has been proposed in the literature (see [6]), but no detailed theoretical analysis of that approach has been carried out so far. As the above mentioned generalization of the T-matrix algorithm turns out to be a linear time-periodic compensator, we will refer to it as the Periodic HHC (PHHC) algorithm. Therefore, both the HHC and the PHHC algorithms call for the use of periodic systems theory ([7]) for closed loop stability and performance analysis. However, a very limited attention has been devoted so far in the literature to the dynamic analysis of vibration attenuation schemes; in particular, the existing contributions to the study of closed loop stability issues (see for example [8]) deal only with time-invariant dynamic models of helicopter dynamics, and the assessment of the role of periodicity in determining the actual closed loop dynamics still has to be fully assessed. More recently, Cheng *et al.* [15] have presented a methodology for the derivation of linearized, time-invariant, state-space models of helicopters and have examined the interaction between HHC and FCS. Finally, it is worthwhile to point out that while HHC and IBC represent significantly different technologies from the implementation point of view (i.e., choice of actuators and sensors), they are completely equivalent from the control theoretic point of view. In particular, the extension of IBC to the more realistic case of a rotor with dissimilar blades requires only a trivial modification of the control algorithms.

In the light of the above remarks, the objectives of this contribution are the following (see also the preliminary results in [9]):

1. to provide a simple state space derivation for the continuous time form of the SISO HHC compensator, first introduced in [3];

2. to demonstrate how the same approach can be used to work out a state space representation for the SISO PHHC compensator, which is suitable for stability and robustness analysis of this kind of rotor control algorithm;

3. to generalize the above results in order to get to a general approach for the derivation of the state space form for a MIMO HHC controller;

4. to present the results of a numerical investigation into the stability properties of Higher Harmonic Control, based on a simulation study of the coupled rotor-fuselage dynamics of a four bladed hingeless rotor helicopter (see [10]).

For the purpose of the present study, only *fixed parameters* HHC will be considered, i.e., the presence of an adaptive part will not be taken into account. Also, the stability analysis is carried out in continuous time. The role of digital implementation on the stability and performance of the HHC loops will be investigated in future work.

Helicopter simulation model

The baseline simulation model used in this study is a nonreal-time, blade element type, coupled rotor-fuselage simulation model (see [10] for details). The fuselage is assumed to be rigid and dynamically coupled with the rotor. A total of nine states describe fuselage motion through the nonlinear Euler equations. Fuselage and blade aerodynamics are described through tables of aerodynamic coefficients, and no small angle assumption is required. A coupled flap-lag-torsion elastic rotor model is used. Blades are modeled as Bernoulli-Euler beams. The rotor is discretized using finite elements, with a modal coordinate transformation to reduce the number of degrees of freedom. The elastic deflections are not required to be small. Blade element theory is used to obtain the aerodynamic characteristics on each blade section. Quasi-steady aerodynamics is used, with a 3-state dynamic inflow model. Linearized models are extracted numerically, by perturbing rotor, fuselage, and inflow states about a trimmed equilibrium position. Since the equations of the coupled rotor/fuselage dynamics are written in the fixed frame of reference, the linearized models turn out to be time-periodic with period T/N, where N is the number of rotor blades and T is the period of one rotor revolution. Note that in the following introducing the azimuth angle $\psi = \Omega t$ will be used as independent variable.

The matrices of the linearized model are generated as Fourier series. For example, the state matrix $A(\psi)$ is given as:

$$A(\psi) = A_0 + \sum_{k=1}^{K} [A_{kc} \cos(kN\psi) + A_{ks} \sin(kN\psi)] \tag{1}$$

where the matrices A_0, A_{kc}, and A_{ks} are constant, and only A_0 is retained for constant coefficient approximations.

Similarly, the control matrix $B(\psi)$ is obtained assuming for the pitch control of each blade the form

$$\begin{aligned}\theta_i(t) = \theta_0 &+ \theta_{1c}\cos(\psi + \frac{2\pi}{N}i) + \theta_{1s}\sin(\psi + \frac{2\pi}{N}i) \\ &+ \theta_{2c}\cos(2\psi + \frac{2\pi}{N}i) + \theta_{2s}\sin(2\psi + \frac{2\pi}{N}i) + \dots \\ &+ \theta_{6c}\cos(6\psi + \frac{2\pi}{N}i) + \theta_{6s}\sin(6\psi + \frac{2\pi}{N}i), \\ &\qquad i = 0, \dots, N-1 \end{aligned} \quad (2)$$

and defining the input vector u of the simulation model as

$$u = \begin{bmatrix}\theta_0 & \theta_{1c} & \theta_{1s} & \dots & \theta_{6c} & \theta_{6s}\end{bmatrix}^T \quad (3)$$

so that in this model the sine and cosine coefficients of the higher harmonics can be used as inputs in the formulation of a vibration control problem.

Finally, the trim procedure is the same as in Ref. [11]. The rotor equations of motion are transformed into a system of nonlinear algebraic equations using a Galerkin method. The algebraic equations enforcing force and moment equilibrium, the Euler kinematic equations, the inflow equations and the rotor equations are combined in a single coupled system. The solution yields the harmonics of a Fourier expansion of the rotor degrees of freedom, the pitch control settings, trim attitudes and rates of the entire helicopter, and main and tail rotor inflow.

State space formulation of higher harmonic controllers

This section presents the state space formulation of HHC controllers of increasing complexity. First, some background on the T-matrix algorithm is given, and a continuous-time, state space analysis is presented for the case of a SISO HHC system in which input and output are at the same harmonic (N/rev, i.e. N times the rotor speed). Next, the analysis is extended to the case in which input and output are at different harmonics and the case of a MIMO HHC system with inputs and outputs at arbitrary harmonics is considered, by combining the results of the two previous cases. More precisely the following three cases, corresponding to three different selections for the control input vector u, will be dealt with:

- Control input given by a single harmonic at the blade passing frequency, i.e.,

$$u = u_N = \begin{bmatrix}\theta_{Nc} & \theta_{Ns}\end{bmatrix}^T$$

- Control input u given by a single harmonic at a frequency different from the blade passing one, i.e.,

$$u = u_M = \begin{bmatrix}\theta_{Mc} & \theta_{Ms}\end{bmatrix}^T$$

with $M \neq N$, like, e.g., $M = N-1$ or $M = N+1$.

- Control input u given by the superposition of a number of different harmonics:

$$u^T = [\theta_{N_1c}\ \theta_{N_1s} \dots \theta_{N_2c}\ \theta_{N_2s} \dots \theta_{N_mc}\ \theta_{N_ms}] \quad (4)$$

with N_i, $i = 1, \dots, m$ multiples of the rotor angular frequency. For example, one might consider in practice the choice of u given by

$$u = \begin{bmatrix}\theta_{(N-1)c}\ \theta_{(N-1)s}\ \theta_{Nc}\ \theta_{Ns}\ \theta_{(N+1)c}\ \theta_{(N+1)s}\end{bmatrix}^T \quad (5)$$

As will be made clear in the following, assuming as control variables the harmonics of the rotating frame pitch control greatly simplifies the task of the state space realization of the HHC compensators.

SISO with input and output at the same frequency

A typical non-adaptive HHC system is based on a discrete time mathematical model describing the response of the helicopter to higher harmonic inputs, of the form

$$y_N(k) = T_{N,N}u_N(k) + y_{0N}(k) \quad (6)$$

where k is the rotor revolution index, y_N is a vector of N/rev harmonics of measured outputs (e.g., hub loads or accelerations at some point of the fuselage), u_N is a vector of control inputs, and $T_{N,N}$ is a 2 by 2 constant matrix. The vector $y_N(k)$ is defined as

$$\begin{aligned} y_N(k) &= \begin{bmatrix} y_{Nc}(k) \\ y_{Ns}(k) \end{bmatrix} \\ &= \begin{bmatrix} \frac{1}{\pi}\int_{k\pi}^{(k+1)\pi} y(\psi)\cos(N\psi)\,d\psi \\ \frac{1}{\pi}\int_{k\pi}^{(k+1)\pi} y(\psi)\sin(N\psi)\,d\psi \end{bmatrix} \end{aligned} \quad (7)$$

The vector y_{0N} contains the N/rev harmonics of the "baseline" vibrations, i.e., the vibrations in the absence of HHC. The control input vector is similarly defined as:

$$u_N = \begin{bmatrix}\theta_{Nc} \\ \theta_{Ns}\end{bmatrix} \quad (8)$$

where θ_{Nc} and θ_{Ns} are, respectively, the cosine and sine components of the N/rev pitch control input, applied in the rotating system.

The HHC inputs are generally updated at discrete time intervals, for example, once per rotor revolution. The conventional HHC control law is derived by minimizing at each discrete time step k the cost function

$$J(k) = y_N(k)^T Q y_N(k) + \Delta u_N(k)^T R \Delta u_N(k) \quad (9)$$

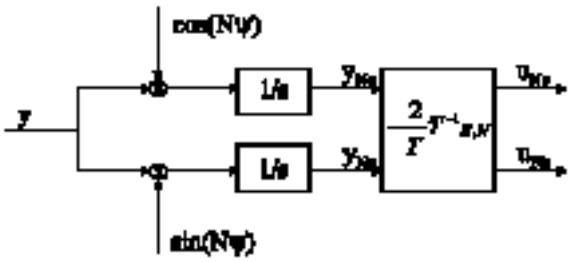

Figure 1: Block diagram of the continuous time SISO HHC algorithm.

where $Q = Q^T \geq 0$, $R > 0$ and $\Delta u_N(k)$ is the increment of the control variable at time k, i.e.,

$$\Delta u_N(k) = u_N(k) - u_N(k-1) \tag{10}$$

Differentiating (9) with respect to $\Delta u_N(k)$ yields the control law

$$u_N(k+1) = u_N(k) - K_{N,N} y_N(k) \tag{11}$$

where $K_{N,N} = (T_{N,N}^T Q T_{N,N} + R)^{-1} T_{N,N}^T Q$. Equation (11) is well known in the literature as the "T-matrix" algorithm. It can be seen from Eqs. (6) and (11) that this control algorithm introduces a discrete time integral action which ensures that $y_N \to 0$ as $k \to \infty$. Actually, with $Q = I_{2,2}$ and $R = 0$ deadbeat control (i.e., the output goes to zero after one discrete-time step) could in principle be achieved if exact knowledge of the $T_{N,N}$ matrix was available, and if the static model, Eq. (6), was an accurate representation of rotor dynamics. However, these two assumptions are generally not satisfied, as $T_{N,N}$ can only be estimated up to some accuracy level and Eq. (6) clearly does not hold if the helicopter is not operating in steady state. Note, also, that if in the cost function (9) one chooses $R = 0$ and Q proportional to the identity matrix, the control law (11) reduces to

$$u_N(k+1) = u_N(k) - T_{N,N}^{-1} y_N(k) \tag{12}$$

which can be given a minimum variance interpretation, in the sense that this control law guarantees at each time step the closed loop minimization of the cost function

$$J(k) = y_N(k)^T y_N(k) \tag{13}$$

Neglecting the effects of the sample and hold scheme of the digital implementation in the T-matrix algorithm, the overall control algorithm can be represented by the block diagram given in Figure 1.

Now, following [3], choose y_{Nc} and y_{Ns} as state variables for the controller in Fig. 1. Then, the following state space model for the HHC compensator is obtained:

$$\dot{y}_N = A_c y_N + B_c(\psi) y \tag{14}$$
$$u = C_c y_N \tag{15}$$

where

$$A_c = \begin{bmatrix} 0 & 0 \\ 0 & 0 \end{bmatrix} \tag{16}$$
$$B_c(\psi) = K_{N,N} \begin{bmatrix} \cos(N\psi) \\ \sin(N\psi) \end{bmatrix} \tag{17}$$
$$C_c = -\frac{2}{T} I_{2,2}$$

SISO with input and output at different frequencies

The HHC input in the rotating system is usually not limited to the same N/rev frequency of the vibrations to be attenuated. Typically, inputs at N-1/rev and N+1/rev are also applied (recall that N/rev inputs of collective, longitudinal, and lateral cyclic pitch in the fixed system result in N-1, N, and N+1/rev pitch inputs in the rotating system).

In this case, the steady state model relating the N/rev harmonic of the output $y(t)$ to the M/rev harmonic of the pitch input $u(t)$, with $M \neq N$, can be written in the form

$$y_N(k) = T_{N,M} u_M(k) + y_{0N}(k) \tag{18}$$

where u_M is defined as in Eq. (8), but for an M/rev harmonic, and where the (constant) matrix $T_{N,M}$ relates the amplitude of the M/rev control input u to the corresponding steady state amplitude of the N/rev component of the output y. The control scheme for the attenuation of N/rev vibrations using an M/rev input can then be derived along the lines of the previous case, and is represented by the equation

$$u_M(k+1) = u_M(k) - K_{N,M} y_N(k) \tag{19}$$

where $K_{N,M} = (T_{N,M}^T Q T_{N,M} + R)^{-1} T_{N,M}^T Q$. As shown in the following Section, the matrix $T_{N,M}$ can be related to the Harmonic Transfer Function (HTF) of the controlled system, which is an extension to periodic systems of the frequency response function of a time-invariant system [12, 13]. In addition, as in the case of HHC with input and output at the same frequency N/rev, the discrete control law, Eq. (19) guarantees that $y_N \to 0$ as $k \to \infty$, provided that the system can be modeled as in Eq. (18).

Similarly to the $M = N$ case, the state space model for the case $N \neq M$ is given by

$$\dot{y}_N = A_c y_N + B_c(\psi) y \tag{20}$$
$$u = C_c y_N \tag{21}$$

where

$$A_c = \begin{bmatrix} 0 & 0 \\ 0 & 0 \end{bmatrix} \tag{22}$$
$$B_c(\psi) = K_{N,M} \begin{bmatrix} \cos(N\psi) \\ \sin(N\psi) \end{bmatrix} \tag{23}$$
$$C_c = -\frac{2}{T} I_{2,2} \tag{24}$$

This discussion shows that a coupled rotor-fuselage system with even a simple SISO HHC controller is intrinsically a system with periodic coefficients if the HHC output and the vibration to be attenuated are at two different multiples of the rotor frequency. This happens even if the rotor-fuselage system is modeled as a system with constant coefficients. Therefore, rigorous stability, performance and robustness analyses of an HHC system can only be carried out using the tools of periodic systems theory.

MIMO with input and output at arbitrary harmonics

In typical implementations of HHC, multi-harmonic signals are frequently used to attenuate several components of the vibratory loads. For example, inputs at N-1/, N/ and N+1/rev, sine and cosine (for a total of 6 inputs), could be used simultaneously to control six components of the N/rev vibratory hub forces and moments. Therefore, this section extends the previous SISO discussion to a MIMO HHC system. We will consider a general configuration in which output measurements of N/rev vibration are available at n different locations, while a number m of harmonics at frequencies N_i, $i = 1, \dots, m$ is applied on the control input u. In this case, the measurement vector has $2n$ elements and is defined as:

$$y_N^T = \begin{bmatrix} y_{Nc}^1 & \dots & y_{Nc}^n & \dots & y_{Ns}^1 & \dots & y_{Ns}^n \end{bmatrix} \quad (25)$$

where y_{Nc}^i and y_{Ns}^i, $i = 1, \dots, n$ are, respectively, the cosine and sine components of the i-th N/rev output, which can be, for example, a force or moment component, or a component of the acceleration at one or more points of the fuselage.

On the other hand, the HHC input vector u has $2m$ elements and is defined as

$$\begin{aligned} u^T &= [u_{N_1c}\, u_{N_1s} \dots u_{N_2c} \\ &\qquad u_{N_2s} \dots u_{N_mc}\, u_{N_ms}] \end{aligned} \quad (26)$$

where u_{N_ic}, $i = 1, \dots, m$ and u_{N_is}, $i = 1, \dots, m$ are the cosine and sine component of the HHC input, at desired harmonics not necessarily equal to N.

Assume now, as in the SISO case, that input and output harmonics are related by the linear equation

$$y_N(k) = \mathbf{T} u(k) + y_{0N}(k) \quad (27)$$

where $\mathbf{T}$ is a $2n \times 2m$ constant coefficient matrix, which is again related to the HTF of the time periodic linearized model of the helicopter. Then, the "T-matrix algorithm" is given by

$$u(k+1) = u(k) - \mathbf{K} y_N(k) \quad (28)$$

where $\mathbf{K} = (\mathbf{T}^T Q \mathbf{T} + R)^{-1} \mathbf{T}^T Q$, where $Q = Q^T \geq 0$ and $R = R^T > 0$ are cost weighting matrices of suitable dimensions.

In the MIMO case, the operation of the HHC control law differs considerably depending on the relationship between the number of control inputs and measured variables which are available. In order to illustrate this, we now consider the formulation of the "T-matrix algorithm" in the MIMO case with $Q = I_{n,n}$ and $R = 0$, by treating separately the cases of $n = m$ and $n > m$[1].

In the case of a "square" control problem, i.e., when $n = m$, the SISO algorithm can be readily extended to

$$u(k+1) = u(k) - \mathbf{T}^{-1} y_N(k) \quad (29)$$

On the other hand, if $n > m$ matrix $\mathbf{T}$ is no longer square and the discrete time control algorithm must be written as

$$u(k+1) = u(k) - \mathbf{T}^{\dagger} y_N(k) \quad (30)$$

where $\mathbf{T}^{\dagger} = (\mathbf{T}^T \mathbf{T})^{-1} \mathbf{T}^T$ is the pseudoinverse of $\mathbf{T}$. In particular, the minimum of the cost function equals zero only in the $n = m$ case, i.e., unless one considers (at least) the square case, it is not possible to guarantee that the vibratory disturbance will be zeroed on all output channels.

The equivalent continuous time formulation for the MIMO HHC compensator, described in discrete form by Eq. (28), can be obtained by applying the previously described SISO results.

Therefore, considering first the case of a control system with as many inputs as outputs, the state-space formulation is given by the order $2n$ system:

$$\dot{y}_N = A_c y_N + B_c(\psi) y \quad (31)$$

$$u = C_c y_N \quad (32)$$

where A_c is the $2n \times 2n$ matrix

$$A_c = \begin{bmatrix} 0 & 0 & \dots & 0 \\ 0 & 0 & \dots & 0 \\ \vdots & \vdots & & \vdots \\ 0 & 0 & \dots & 0 \end{bmatrix} \quad (33)$$

$B_c(\psi)$ is the $2n \times n$ matrix

$$B_c(\psi) = \mathbf{K} \begin{bmatrix} \cos(N\psi) I_{n,n} \\ \sin(N\psi) I_{n,n} \end{bmatrix} \quad (34)$$

and

$$C_c = -\frac{2}{T} I_{2n \times 2n} \quad (35)$$

For example, consider the case of a control system relying on the application of (N-1), N and (N+1)/rev inputs in the rotating frame in order to attenuate vibratory accelerations in $n = 3$ different locations in the fuselage,

[1] The case of $n < m$ is hardly relevant from a practical point of view.

so that $m = 3$, $N_1 = N - 1$, $N_2 = N$ and $N_3 = N + 1$ and

$$u^T = \left[\theta_{(N-1)c}\ \theta_{(N-1)s}\ \theta_{Nc}\ \theta_{Ns}\ \theta_{(N+1)c}\ \theta_{(N+1)s}\right] \quad (36)$$

$$y^T = [y_1\ y_2\ y_3] \quad (37)$$

Then, the state space model for the controller is given by

$$A_c = 0_{6\times 6} \quad (38)$$

$$B_c(\psi) = \mathbf{K}\begin{bmatrix} \cos(N\psi) & 0 & 0 \\ 0 & \cos(N\psi) & 0 \\ 0 & 0 & \cos(N\psi) \\ \sin(N\psi) & 0 & 0 \\ 0 & \sin(N\psi) & 0 \\ 0 & 0 & \sin(N\psi) \end{bmatrix} \quad (39)$$

As in the SISO case, since the control inputs are directly given by the higher harmonics of θ, there is no need for a "modulation" term in matrix C_c which therefore turns out to be constant:

$$C_c = -\frac{2}{T} I_{6\times 6} \quad (40)$$

Similar expressions can be worked out in the case of a control system with more outputs than inputs.

Definition of the T matrix in terms of the helicopter models

The control laws discussed in the previous Section call for the availability of input/output models for the helicopter response to higher harmonic control inputs. The objective of this Section is to provide the necessary background on the frequency response of time-periodic systems and use such analytical tools in order to derive explicit expressions for the T matrix.

Development of the Harmonic Transfer Function

This Section summarizes the main aspects of the development of the Harmonic Transfer Function (HTF) [12]. Consider a continuous-time linear periodic system:

$$\begin{aligned} \dot{x}(t) &= A(t)x(t) + B(t)u(t) \\ y(t) &= C(t)x(t) + D(t)u(t) \end{aligned} \quad (41)$$

Each matrix can be expanded in a complex Fourier series

$$A(t) = \sum_{m=-\infty}^{\infty} A_m e^{jm\Omega t} \quad (42)$$

and similarly for $B(t)$, $C(t)$ and $D(t)$. The system can be analyzed in the frequency domain as follows. Introduce the class of *Exponentially Modulated Periodic* (EMP) signals [12]. The (complex) signal $u(t)$ is said to be EMP of period T and modulation s if

$$u(t) = \sum_{k=-\infty}^{\infty} u_k e^{s_k t} = e^{st} \sum_{k=-\infty}^{\infty} u_k e^{jk\Omega t} \quad (43)$$

where $t \geq 0$, $s_k = s + jk\Omega$, and s is a complex scalar.

The class of EMP signals is a generalization of the class of T-periodic signals, i.e., of signals with period T: in fact, an EMP signal with $s = 0$ is just an ordinary time-periodic signal.

In much the same way as a time invariant system subject to a (complex) exponential input has an exponential steady-state response, a periodic system subject to an EMP input has an EMP steady-state response. In such a response, all signals of interest (x, $\dot{x}$, y) can be expanded as EMP signals. By deriving Fourier expansions for $A(t)$, $B(t)$, $C(t)$ and $D(t)$, it is possible to prove that the EMP steady-state response of the system can be expressed as the infinite dimensional matrix equation with *constant* elements [12]

$$\begin{aligned} s\mathcal{X} &= (\mathcal{A} - \mathcal{N})\mathcal{X} + \mathcal{B}\mathcal{U} \\ \mathcal{Y} &= \mathcal{C}\mathcal{X} + \mathcal{D}\mathcal{U} \end{aligned} \quad (44)$$

where $\mathcal{X}$, $\mathcal{U}$ and $\mathcal{Y}$ are doubly infinite vectors formed with the harmonics of x, u and y respectively, organized in the following fashion:

$$\mathcal{X}^T = \left[\cdots\ x_{-2}^T\ x_{-1}^T\ x_0^T\ x_1^T\ x_2^T\ \cdots\right] \quad (45)$$

and similarly for $\mathcal{U}$ and $\mathcal{Y}$. $\mathcal{A}$, $\mathcal{B}$, $\mathcal{C}$ and $\mathcal{D}$ are doubly infinite Toeplitz matrices formed with the harmonics of $A(\cdot)$, $B(\cdot)$, $C(\cdot)$ and $D(\cdot)$ respectively as follows

$$\mathcal{A} = \begin{bmatrix} \ddots & \vdots & \vdots & \vdots & \vdots & \vdots & \\ \cdots & A_0 & A_{-1} & A_{-2} & A_{-3} & A_{-4} & \cdots \\ \cdots & A_1 & A_0 & A_{-1} & A_{-2} & A_{-3} & \cdots \\ \cdots & A_2 & A_1 & A_0 & A_{-1} & A_{-2} & \cdots \\ \cdots & A_3 & A_2 & A_1 & A_0 & A_{-1} & \cdots \\ \cdots & A_4 & A_3 & A_2 & A_1 & A_0 & \cdots \\ & \vdots & \vdots & \vdots & \vdots & \vdots & \ddots \end{bmatrix} \quad (46)$$

(and similarly for $\mathcal{B}$, $\mathcal{C}$ and $\mathcal{D}$), where the submatrices A_n in Eq. (46) are the coefficients of the Fourier expansion of matrix $A(t)$, given in Eq. (42). Note that the expansions of the state space matrices can be also expressed in trigonometric form, see Eq. (1), as follows [2]

$$\begin{aligned} A_k &= \tfrac{1}{2}(A_{kc} - jA_{ks}) \\ & \qquad k = 1, 2, \ldots \\ A_{-k} &= \tfrac{1}{2}(A_{kc} + jA_{ks}) \end{aligned} \quad (47)$$

[2] Recall that the Fourier series can be rewritten in complex exponential form, i.e., $a(t) = a_0 + \sum_{k=1}^{\infty}(a_{nc}\cos n\omega t + a_{ns}\sin n\omega t) = \sum_{k=-\infty}^{\infty} a_k e^{jk\omega t}$, with $a_k = (a_{kc} - ja_{ks})/2$, and $a_{-k} = (a_{kc} + ja_{ks})/2, k = 1, 2, \ldots$

with A_0 identical in both Eq. (46) and Eq. (1). Similar relations hold for the harmonics of B, C, and D.

Matrix $\mathcal{N}$ is a block diagonal complex-valued matrix given by

$$\begin{aligned}\mathcal{N} &= \text{blkdiag}\{jn\Omega I\} = \\ &= j\Omega \begin{bmatrix} \ddots & \vdots & \vdots & \vdots & \vdots & \vdots & \\ \cdots & -2I & 0 & 0 & 0 & 0 & \cdots \\ \cdots & 0 & -I & 0 & 0 & 0 & \cdots \\ \cdots & 0 & 0 & 0 & 0 & 0 & \cdots \\ \cdots & 0 & 0 & 0 & I & 0 & \cdots \\ \cdots & 0 & 0 & 0 & 0 & 2I & \cdots \\ & \vdots & \vdots & \vdots & \vdots & \vdots & \ddots \end{bmatrix}\end{aligned} \tag{48}$$

where I is the identity matrix, of size equal to the number of states.

From Eq. (44), one can define the HTF as the operator:

$$\mathcal{G}(s) = \mathcal{C}[s\mathcal{I} - (\mathcal{A} - \mathcal{N})]^{-1}\mathcal{B} + \mathcal{D} \tag{49}$$

which relates the input harmonics and the output harmonics (contained in the infinite vectors $\mathcal{U}$ and $\mathcal{Y}$ respectively). Eq. (49) is the extension to the case of periodic systems of the corresponding constant coefficient expression for the transfer function

$$G(s) = C\left[sI - A\right]^{-1} B + D \tag{50}$$

In particular, if $s = 0$, which, in the helicopter case, corresponds to the steady-state response of the system to a periodic input of basic frequency N/rev, the appropriate input/output operator for periodic systems becomes

$$\mathcal{G}(0) = \mathcal{C}[\mathcal{N} - \mathcal{A}]^{-1}\mathcal{B} + \mathcal{D} \tag{51}$$

Definition of the T matrix

The $T_{N,N}$, $T_{N,M}$ and $\mathbf{T}$ matrices used in the formulation of the HHC and PHHC algorithms can be related to the elements of the HTF of the linearized helicopter model, as follows.

First of all, note that according to the definition of the control input vector u which has been adopted, the rotor will be subject to a proper, steady state higher harmonic control input whenever the control vector u is *constant*. This implies that in order to define the T matrix for the helicopter we only have to study the response of the periodic helicopter models to a EMP input with $s = 0$, i.e., we only have to compute the input/output operator $\hat{\mathcal{G}}(0)$. For example, consider the linear time-periodic system (41) and the constant input $u(t) = u_0$. The vector $\mathcal{U}$ corresponding to $u(t) = u_0$ is given by

$$\mathcal{U}^T = \left[\cdots \;\; 0 \;\; 0 \;\; u_0^T \;\; 0 \;\; 0 \;\; \cdots\right] \tag{52}$$

and the steady state response $\mathcal{Y}$ of the periodic system is given by

$$\mathcal{Y} = \mathcal{G}(0)\mathcal{U} \tag{53}$$

which can be equivalently written as

$$\begin{bmatrix} \vdots \\ y_{-2N} \\ y_{-N} \\ y_0 \\ y_N \\ y_{2N} \\ \vdots \end{bmatrix} = \begin{bmatrix} \ddots & \vdots & \vdots & \\ \cdots & G_{-2N,-2N} & G_{-2N,-N} & \\ \cdots & G_{-N,-2N} & G_{-N,-N} & \\ \cdots & G_{0,-2N} & G_{0,-N} & \\ \cdots & G_{N,-2N} & G_{N,-N} & \\ \cdots & G_{2N,-2N} & G_{2N,-N} & \\ & \vdots & \vdots & \end{bmatrix}$$
$$\begin{bmatrix} \vdots & \vdots & \vdots & \\ G_{-2N,0} & G_{-2N,N} & G_{-2N,2N} & \cdots \\ G_{-N,0} & G_{-N,N} & G_{-N,2N} & \cdots \\ G_{0,0} & G_{0,N} & G_{0,2N} & \cdots \\ G_{N,0} & G_{N,N} & G_{N,2N} & \cdots \\ G_{2N,0} & G_{2N,N} & G_{2N,2N} & \cdots \\ \vdots & \vdots & \ddots & \end{bmatrix} \begin{bmatrix} \vdots \\ 0 \\ 0 \\ u_0 \\ 0 \\ 0 \\ \vdots \end{bmatrix} \tag{54}$$

From equation (54) we have that

$$\begin{bmatrix} y_{-N} \\ y_N \end{bmatrix} = \begin{bmatrix} G_{-N,0} \\ G_{N,0} \end{bmatrix} u_0 \tag{55}$$

and converting the N/rev harmonics of the output from exponential to trigonometric form we have that[3]

$$\begin{bmatrix} y_{Nc} \\ y_{Ns} \end{bmatrix} = 2 \begin{bmatrix} \text{Real}[G_{N,0}] \\ \text{Imag}[G_{N,0}] \end{bmatrix} u_0, \tag{56}$$

so that the T matrix is given by

$$\mathbf{T} = 2 \begin{bmatrix} \text{Real}[G_{N,0}] \\ \text{Imag}[G_{N,0}] \end{bmatrix} \tag{57}$$

Construction of the T matrix

From a practical point of view, the above theoretical analysis of the frequency response of periodic system, and the corresponding definitions for the T-matrix relating selected input-output frequencies only, rely on the use of infinite dimensional matrices. When it comes to the numerical construction of the T-matrix, however, one has to resort to finite dimensional approximations of the system matrices $\mathcal{A}$, $\mathcal{B}$, $\mathcal{C}$, and $\mathcal{D}$. Consider, for example, the problem of constructing the T-matrix, as defined in equation (57) for a periodic system of the form (41) with n outputs, m inputs and n_s states. First of all, one chooses the dimension of the expansions $\mathcal{A}$, $\mathcal{B}$, $\mathcal{C}$, and $\mathcal{D}$ for the state space matrices A, B, C, and D, in terms of the number of block rows one wants to take into account in $\mathcal{A}$. For example, we choose to include a number $B = 5$ of blocks in each row of the expansion of the system matrices, then $\mathcal{A}$ has dimension $n_sB \times n_sB$

[3] Note that $G_{-N,0}$ and $G_{N,0}$ are complex conjugate.

and is given by

$$\mathcal{A} = \begin{bmatrix} A_0 & A_{-1} & A_{-2} & A_{-3} & A_{-4} \\ A_1 & A_0 & A_{-1} & A_{-2} & A_{-3} \\ A_2 & A_1 & A_0 & A_{-1} & A_{-2} \\ A_3 & A_2 & A_1 & A_0 & A_{-1} \\ A_4 & A_3 & A_2 & A_1 & A_0 \end{bmatrix} \tag{58}$$

and similarly for $\mathcal{B}$, $\mathcal{C}$, and $\mathcal{D}$. Therefore, the HTF is given by the $2nB \times mB$ matrix, as follows

$$\begin{bmatrix} y_{-2N} \\ y_{-N} \\ y_0 \\ y_N \\ y_{2N} \end{bmatrix} = \mathcal{G}(0)\mathcal{U}$$

$$= \begin{bmatrix} G_{-2N,-2N} & G_{-2N,-N} \\ G_{-N,-2N} & G_{-N,-N} \\ G_{0,-2N} & G_{0,-N} \\ G_{N,-2N} & G_{N,-N} \\ G_{2N,-2N} & G_{2N,-N} \end{bmatrix} \begin{bmatrix} G_{-2N,0} & G_{-2N,N} & G_{-2N,2N} \\ G_{-N,0} & G_{-N,N} & G_{-N,2N} \\ G_{0,0} & G_{0,N} & G_{0,2N} \\ G_{N,0} & G_{N,N} & G_{N,2N} \\ G_{2N,0} & G_{2N,N} & G_{2N,2N} \end{bmatrix} \begin{bmatrix} 0 \\ 0 \\ u_0 \\ 0 \\ 0 \end{bmatrix} \tag{59}$$

Using a Matlab-like notation, the blocks $G_{-N,0}$, $G_{N,0}$ can be extracted from $\mathcal{G}(0)$ as the submatrices $\mathcal{G}(0)(2n+1:3n, 2m+1:3m)$ and $\mathcal{G}(0)(4n+1:5n, 2m+1:3m)$. respectively. Clearly, the choice of the number of block rows B will affect the accuracy of the numerical construction (see also [14] for an analysis of the effect of truncation in the study of frequency response operators), so as a general rule B should be chosen sufficiently large in order to ensure that the T-matrix constructed from the truncated HTF gives a good approximation of the actual T-matrix.

Formulation of the coupled helicopter/HHC model

The compensator will be designed along the lines of Ref. [12]. Denote with $A(\psi)$, $B(\psi)$, $C(\psi)$, and $D(t)$ the matrices for the LTP state space model of the helicopter, for the selected input/output pair. Similarly, denote with $A_c(\psi)$, $B_c(\psi)$, $kC_c(\psi)$ the compensator's state space model. The closed-loop LTP state matrix $A_e(\psi)$ is given by

$$A_e(\psi) = \begin{bmatrix} A(\psi) & B(\psi)C_c \\ B_c(\psi)C(\psi) & Ac + B_c(\psi)D(\psi)C_c \end{bmatrix} \tag{60}$$

The closed-loop stability of the helicopter with HHC is then given by the characteristic exponents of $A_e(\psi)$, and will be studied as a function of the design parameters Q and R. In practice $A_e(\psi)$ is computed directly by linearizing the nonlinear closed-loop system equations.

Results

The objective of this Section is to present the results obtained in the stability analysis of a Higher Harmonic Control loop which has been designed on the basis of a coupled rotor-fuselage simulation model. Note that for the purpose of this study a continuous time implementation of the controller is assumed, i.e., the analysis is carried out by using the continuous time state space form for the HHC controllers derived in the previous Sections. Discretization issues will be analyzed in future work.

The helicopter configuration used for the present study is similar to the Eurocopter B0-105, with a thrust coefficient $C_T/\sigma = 0.071$. Three blade modes are used in the modal coordinate transformation, namely, the fundamental flap, lag, and torsion modes, with a natural frequency of 1.12/rev, 0.7/rev, and 3.4/rev, respectively. Because the aerodynamic model consists of a simple linear inflow with quasi-steady aerodynamics, vibratory loads and CG accelerations, and consequently also IBC inputs, tend to be underestimated. Therefore, their absolute values can be considered representative only in a qualitative sense. However, the overall simulation model is likely reasonable for stability studies, and for a general assessment of the design and closed-loop analysis methodology.

In all cases, the helicopter is first trimmed in steady, straight flight, at the desired velocity. Then, the nonlinear simulation begins, with the pilot controls held fixed at their trim values, and the IBC system turned on at time $t = 0$.

Results for V=80 kts

Figures 2 and 3 show, respectively, peak-to-peak magnitude and phase of the 4/rev component of the vertical (i.e., along the z-body axis) acceleration at the CG, for a speed $V = 80$ kts, corresponding to $\mu = 0.19$. The figures show four curves, one each for values of r=0, 10, 100, and 1000. The high-frequency oscillations visible in the curves of these, and of many subsequent figures, are largely an artifact of the numerical procedure used to extract the 4/rev magnitude and phase from the time histories of the accelerations. Clearly, the IBC system is very effective, and reduces in a few seconds the 4/rev vertical acceleration to a small fraction of its trim value in just a few seconds.

The vibration attenuation is also very clear for the CG roll acceleration $\dot{p}$: magnitude and phase of the 4/rev components are shown in Figures 4 and 5, respectively. Magnitude and phase of the 4/rev components of the roll acceleration $\dot{q}$ are shown in Figures 6 and 7, respectively. Both $\dot{p}$ and $\dot{q}$ are reduced to 5% or less of their trim values in no more than 6-7 seconds.

Magnitudes and phases of the IBC inputs are presented in Figs. 8 through 11. Figures 8 and 9 show magnitude and phase of the 3/, 4/, and 5/rev components for the case $r = 0$, i.e., no restrictions on the control effort. Figures 10 and 11 show magnitude and phase for

the case $r = 1000$. Comparing the two sets of results, it can be seen that the controls reach their steady-state values much more quickly for the case $r = 0$ than for $r = 1000$. In the latter case, the steady-state values of θ_3 and θ_5 have not yet been reached at the end of 7 sec of simulation.

It is interesting to note that the action of the IBC system, and the consequent vibration reduction, occurs within times of the order of 5-7 sec or, equivalently, of about 1 rad/sec. These are also typical time scales for flight control systems, and also overlap typical piloting frequencies. Therefore, the results previously shown indicate the possibility of interaction with the stability and control characteristics of the helicopter.

It is also interesting to consider the closed-loop poles of the system. Computation of the closed-loop state matrix A_e was achieved by linearizing the augmented nonlinear set of equations. Figure 12 shows a root locus plot of just the controller poles for increasing values of r, using a constant coefficient approximation to A_e. The system displays an unstable complex conjugate pair at 80 knots, but there is no trace of the instability in the closed-loop simulations using the full nonlinear system, previously shown. The instability is probably due to the errors made in modeling the periodic system with a constant coefficient approximation. In fact, when the periodicity is fully taken into account, the instability disappears. This can be seen in Fig. 13, which shows the real parts of the characteristic exponents of the least damped modes, using Floquet theory. None of the modes, which include controller, rotor, and rigid body modes, becomes unstable for any of the values of r considered. This confirms that, whenever the IBC input includes harmonics that are different from the harmonic that one is trying to attenuate, the closed-loop problem is intrinsically time-periodic. Constant coefficient approximations may not yield correct correct closed-loop stability results, as in this case, even at lower advance ratios, where constant coefficient approximations give acceptable results for the open-loop system.

Finally, the position of the poles appears to be linked to the vibration reduction performance. In general, for the highest control effort (tuning parameter $r = 0.0$) controller poles tend to be farther away from the origin, and as r increases they come closer to it.

Results for V=140 and 170 kts

Figures 14 through 19 show the 4/rev CG acceleration components at a speed of V=140 kts, corresponding to an advance ratio $\mu = 0.33$. Magnitude and phase of the vertical acceleration are shown in Fig. 14 and 15, respectively. The IBC is extremely effective, and reduces the magnitude of the 4/rev accelerations to almost zero within about 7 seconds. Near-perfect attenuation of the roll acceleration $\dot{p}$ can be seen in Fig. 16. The apparent large phase changes of the 4/rev component of $\dot{p}$ that appear in Fig. 17 are indeed a numerical artifact, due to the fact that the calculation of the phase is carried out on numbers that are very near to zero. Finally, Figs. 18 and 19 show magnitude and phase of the 4/rev component of the pitch acceleration $\dot{q}$, which is also very well attenuated by the IBC system.

Magnitude and phase of the corresponding values of the 3/, 4/, and 5/rev inputs are shown in Fig. 20 and 21, respectively, for the case $r = 0$. The steady-state values of each control are reached in about 7 seconds, therefore the time scale of action of the controller is approximately the same as in the 80 kts case. The magnitudes and phases of the input for the case $r = 1000$ are shown in Figs. 22 and 23 respectively. Differently from the 80 kts case, the control time histories for $r = 0$ and $r = 1000$ are very similar.

The LTI, closed-loop poles for V=140 kts are shown in Fig. 24. At this speed, all the poles are stable, with the partial exception of a complex controller poles, that is unstable but extremely close to the origin.

Finally, one result for the case V=170 kts, corresponding to $\mu = 0.4$. Note that the simulation cannot compute a trim state at this speed. Therefore, the drag of the fuselage was arbitrarily reduced until a trimmed state was achieved. Figure 25 shows baseline and IBC-on magnitudes of the 4/rev component of the vertical acceleration. Again, the IBC is very effective at attenuating vibrations, and the attenuation occurs on the same time scales as for the speeds previously shown. Additional results were obtained for this speed, but are not presented here for reasons of space. However, the overall trends are the same as seen for the V=80 kts and V=140 kts cases. The closed-loop LTI system is stable.

Summary and conclusions

The present paper summarized the simple state space derivation for the continuous time form of the SISO HHC compensator; demonstrated how the same approach can be used to work out a state space representation for the SISO PHHC compensator, which is suitable for stability and robustness analysis; generalized that result in order to get to a general approach for the derivation of the state space form for a MIMO HHC controller; and presented the results of a numerical investigation into the performance and stability properties of Higher Harmonic Control, implemented in the rotating system, based on a simulation study of the coupled rotor-fuselage dynamics of a four bladed hingeless rotor helicopter.

The results of the simulation study indicate that

1. The IBC controller is very effective in reducing the desired components of the 4/rev CG accelerations. Because the aerodynamic model used leads to underestimating these vibratory components, the absolute values of the reduction and of the control inputs may not be fully reliable. However, the percentage reductions obtained in the simulations are in excess of 80-90%.

2. The vibration attenuation occurs within 5-7 seconds after the IBC system is turned on. This is equivalent to a frequency of around 1 rad/sec, which is a frequency at which flight control systems and human pilots can operate. Therefore, the interactions and potential adverse effects on the stability and control characteristics of the helicopter should be explored.

3. The IBC problem is intrinsically time-periodic if the IBC inputs include frequencies other than the frequency one wishes to attenuate. This is true even if the rest of the model is assumed to be time-invariant. In these cases, the closed-loop stability results obtained using a constant coefficient approximations may be incorrect even at lower values of the advance ratio μ, where constant coefficient approximation of the open-loop dynamics are accurate.

Acknowledgments

This research was supported by the U.S. Army Research Office, under the grant 41569-EG, Technical Monitor Dr. Gary Anderson.

References

[1] Friedmann, P.P., and Millott, T., "Vibration Reduction in Rotorcraft Using Active Control-A Comparison of Various Approaches," *Journal of Guidance, Control and Dynamics*, Vol. 18, No. 4, Jul-Aug 1995, pp. 664-673.

[2] Teves, D., Niesl, G., Blaas, A., and Jacklin, S., "The Role of Active Control in Future Rotorcraft," Paper III.10.1–17, *Proceedings of the 21st European Rotorcraft Forum*, Saint Petersburg, Russia, Sept 1995.

[3] Wereley, N., and Hall, S., "Linear Control Issues in the Higher Harmonic Control of Helicopter Vibrations," *Proceedings of the 45th Forum of the American Helicopter Society*, Boston, MA, May 1989.

[4] Shaw, J., and Albion, N, "Active Control of the Helicopter Rotor for Vibration Reduction," *Journal of the American Helicopter Society*, Vol. 26, 1981.

[5] Johnson, W., *Helicopter theory*, Princeton University Press, 1980.

[6] Muller, M., Arnold, U. T. P., and Morbitzer, D., "On the Importance and Effectiveness of 2/rev IBC for Noise, Vibration and Pitch Link Load Reduction," *Proceedings of the 55th Anual Forum of the American Helicopter Society*, 2000.

[7] Bittanti, S., and Colaneri, P., "Periodic control," in J.G. Webster, editor, *Wiley Encyclopedia of Electrical and Electronic Engineering*, John Wiley and Sons, 1999.

[8] Du Val, R., Gregory, C., and Gupta, N., "Design and Evaluation of a State Feedback Vibration Controller," *Journal of the American Helicopter Society*, Vol. 29, 1984, pp. 30-37.

[9] Lovera, M., Colaneri, P., and Celi, R., "Periodic Analysis of Higher Harmonic Control Techniques for Helicopter Vibration Attenuation," *Proceedings of the 2003 American Control Conference*, Denver, Colorado, 2003

[10] Theodore, C., and Celi, R., "Helicopter Flight Dynamic Simulation with Refined Aerodynamic and Flexible Blade Modeling," *Journal of Aircraft*, Vol. 39, No. 4, Jul-Aug 2002, pp. 577-586.

[11] Celi, R., "Hingeless Rotor Dynamics in Coordinated Turns," *Journal of the American Helicopter Society*, Vol. 36, No. 4, Oct 1991, pp. 39-47.

[12] Wereley, N., and Hall, S. "Frequency Response of Linear Time Periodic Systems," *Proceedings of the 29th IEEE Conference on Decision and Control*, 1990, pp. 3650-3655.

[13] D'Angelo, H., *Linear Time-Varying Systems: Analysis and Synthesis*, Allyn and Bacon, 1970.

[14] Zhou, J., and Hagiwara, T., "H_2 and H_∞ Norm Computations of Linear Continuous-Time Periodic Systems Via the Skew Analysis of Frequency Response Operators," *Automatica*, Vol. 38, No. 8, 2002, pp. 1381-1387.

[15] Cheng, R. P., Tischler, M. B., and Celi, R., "A High-Order, Time Invariant Linearized Model for Application to HHC/AFCS Interaction Studies," *Proceedings of the 59th Annual Forum of the American Helicopter Society*, Phoenix, AZ, May 2003.

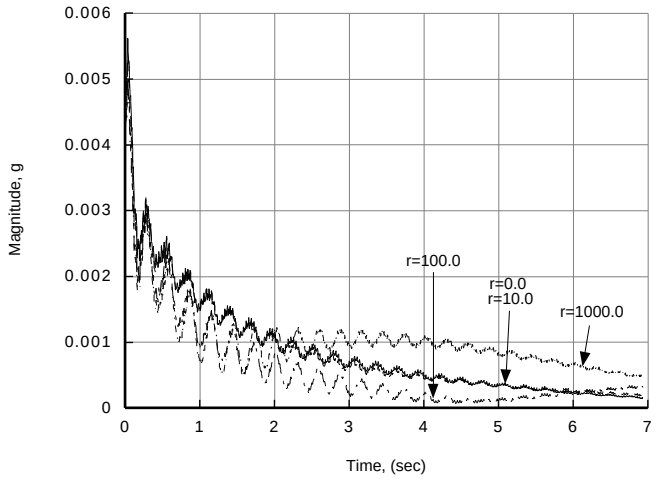

Figure 2: Peak-to-peak 4/rev vertical accelerations at helicopter CG in g for 80 kts ($\mu = 0.188$).

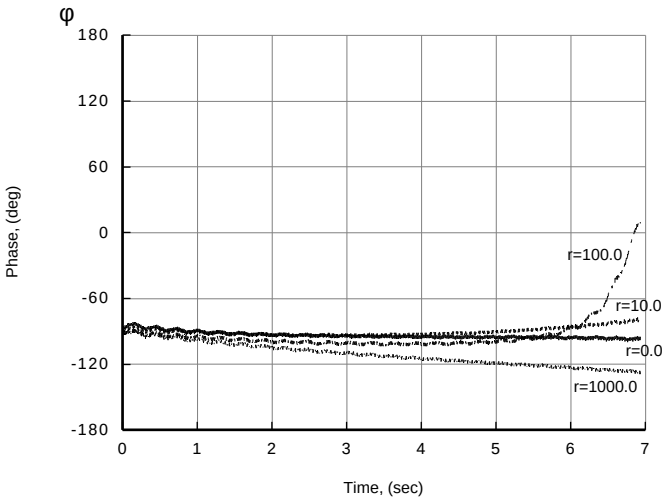

Figure 5: Phase of 4/rev roll accelerations of helicopter for 80 kts ($\mu = 0.188$).

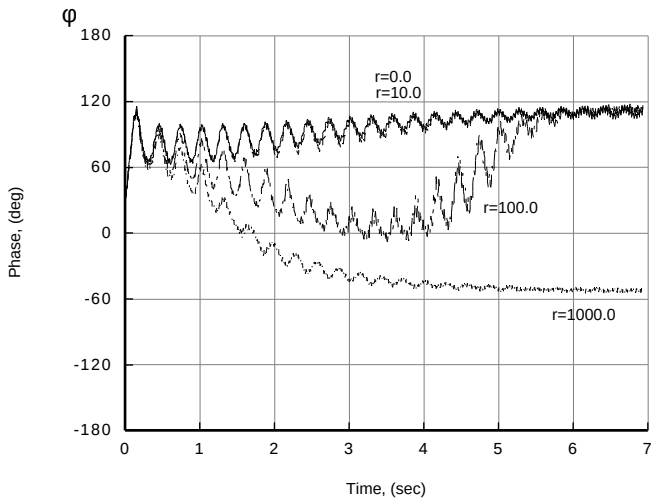

Figure 3: Phase in degrees of the 4/rev vertical accelerations at helicopter CG for 80 kts ($\mu = 0.188$).

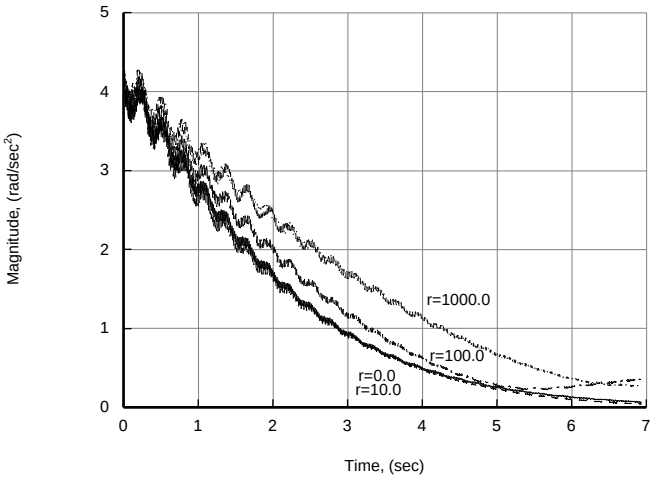

Figure 6: Peak-to-peak 4/rev pitch accelerations of helicopter for 80 kts ($\mu = 0.188$).

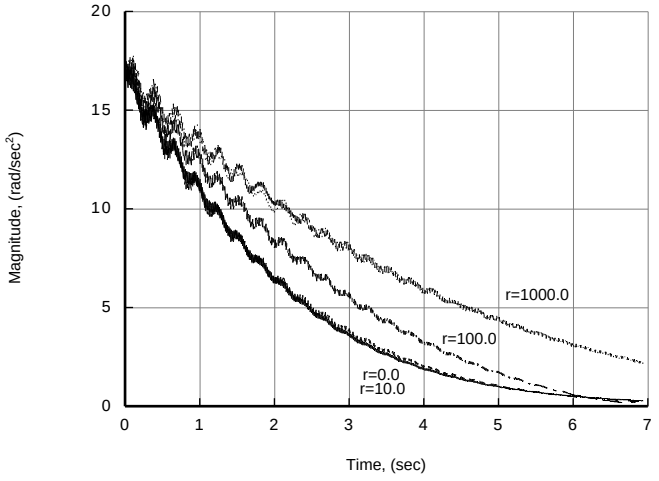

Figure 4: Peak-to-peak 4/rev roll accelerations of helicopter for 80 kts ($\mu = 0.188$).

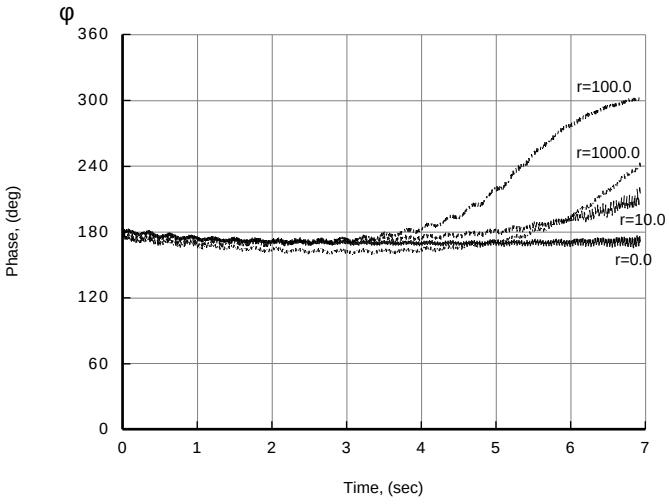

Figure 7: Phase of 4/rev pitch accelerations of helicopter for 80 kts ($\mu = 0.188$).

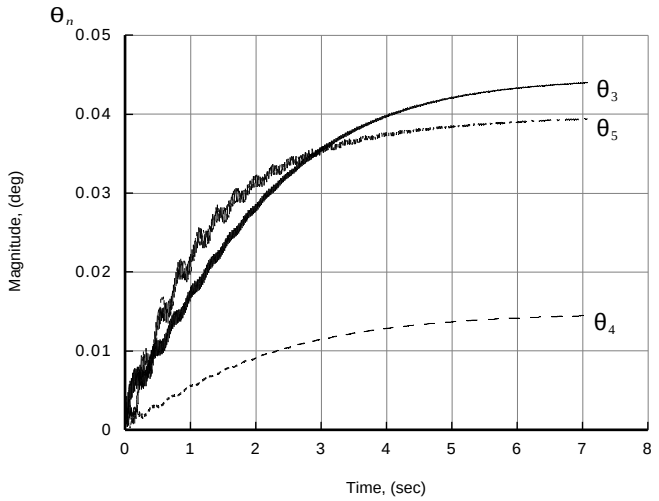

Figure 8: IBC/HHC control input amplitude in degrees, 80 kts ($\mu \approx 0.189$) and r=0.0.

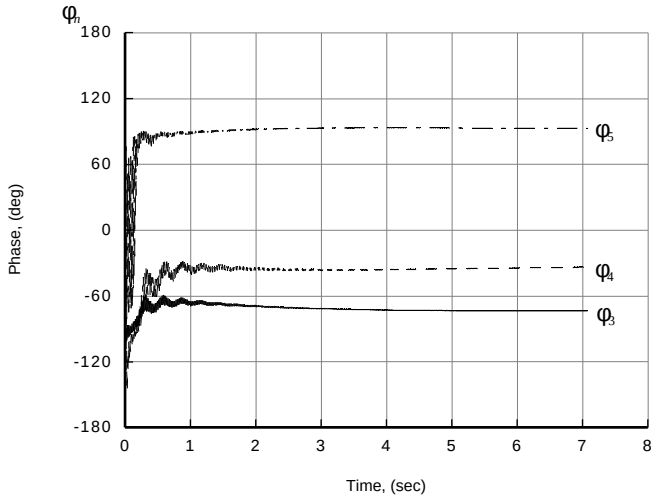

Figure 9: IBC/HHC control input phase in degrees, 80 kts ($\mu \approx 0.189$) and r=0.0.

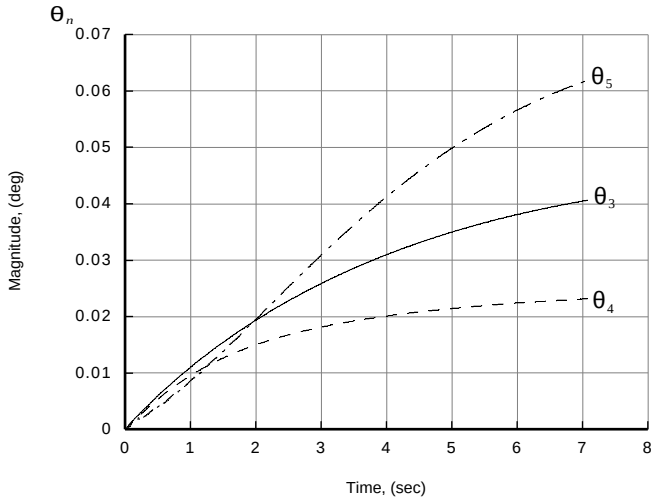

Figure 10: IBC/HHC control input amplitude in degrees, 80 kts ($\mu \approx 0.189$) and r=1000.0.

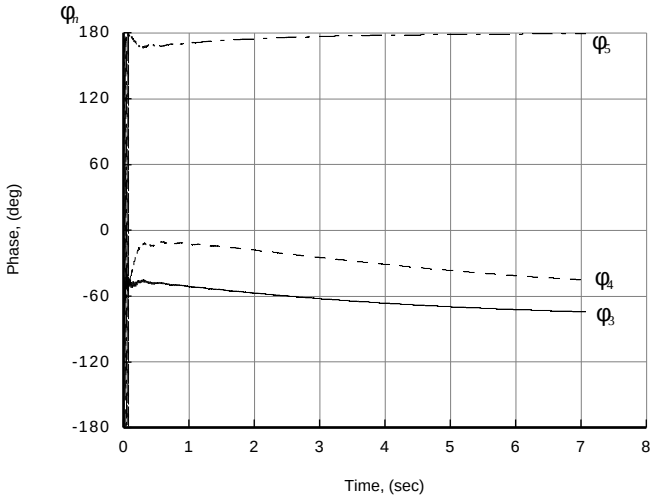

Figure 11: IBC/HHC control input phase in degrees, 80 kts ($\mu \approx 0.189$) and r=1000.0.

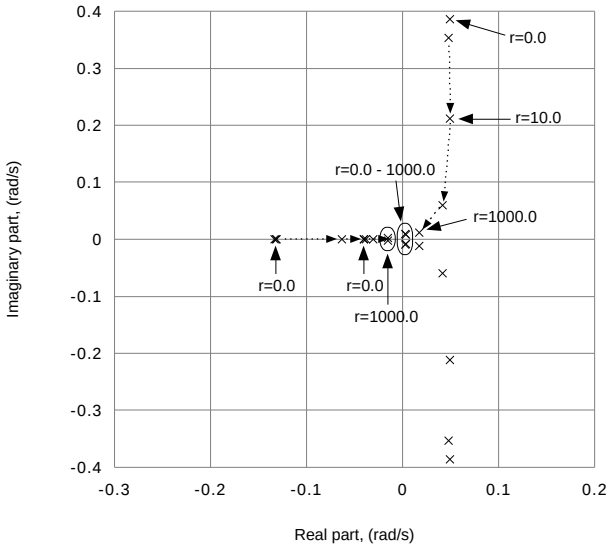

Figure 12: Root-locus of LTI closed-loop system controller poles, 80 kts.

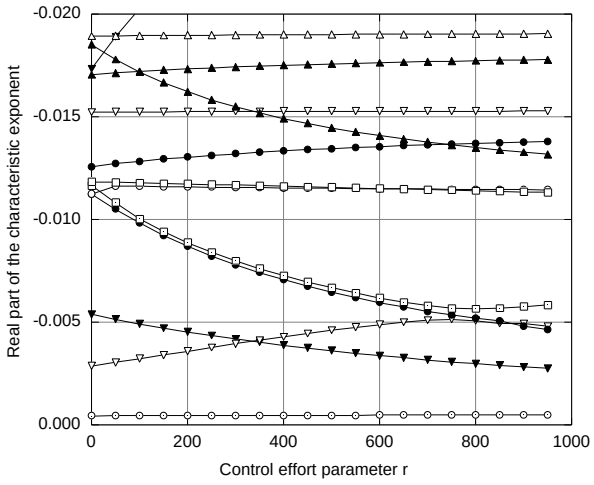

Figure 13: Real parts of the characteristic exponents of the least damped modes, 80 kts.

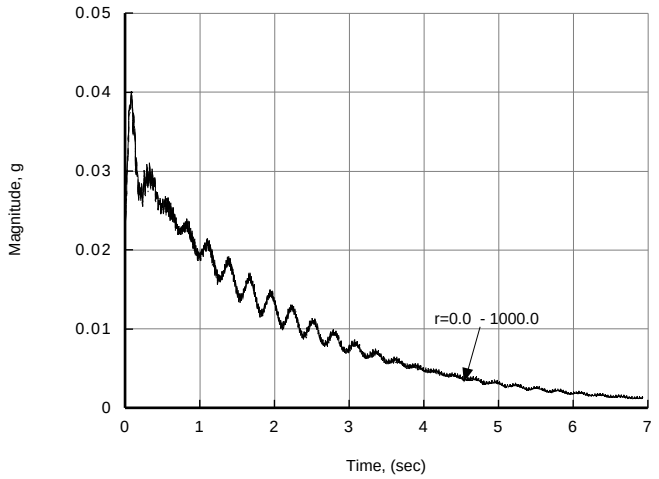

Figure 14: Peak-to-peak 4/rev vertical accelerations at helicopter CG in g for 140 kts ($\mu = 0.330$).

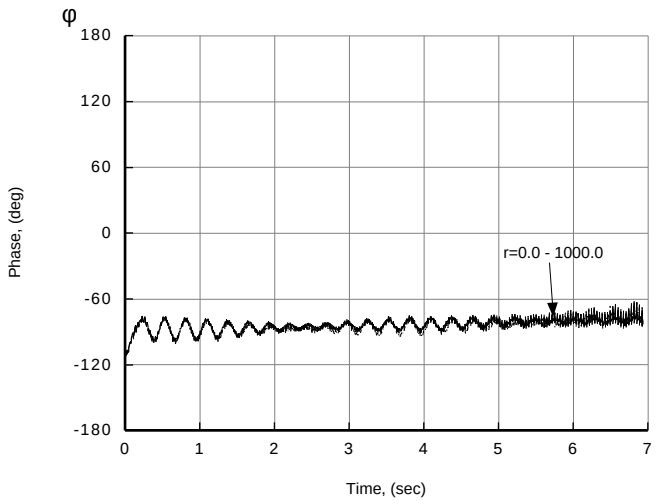

Figure 15: Phase in degrees of the 4/rev vertical accelerations at helicopter CG for 140 kts ($\mu = 0.330$).

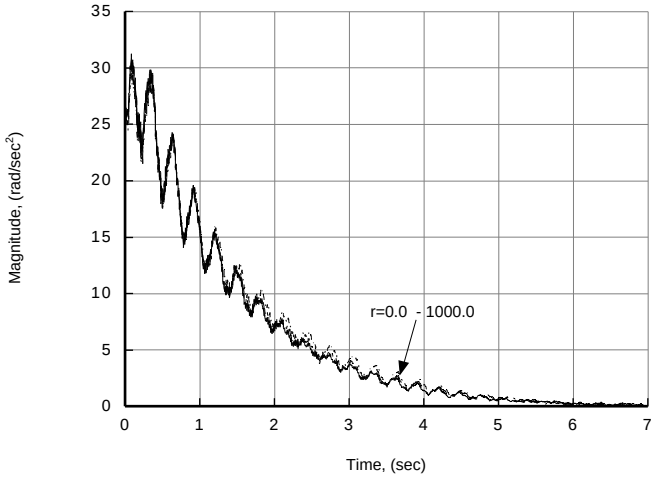

Figure 16: Peak-to-peak 4/rev roll accelerations of helicopter for 140 kts ($\mu = 0.330$).

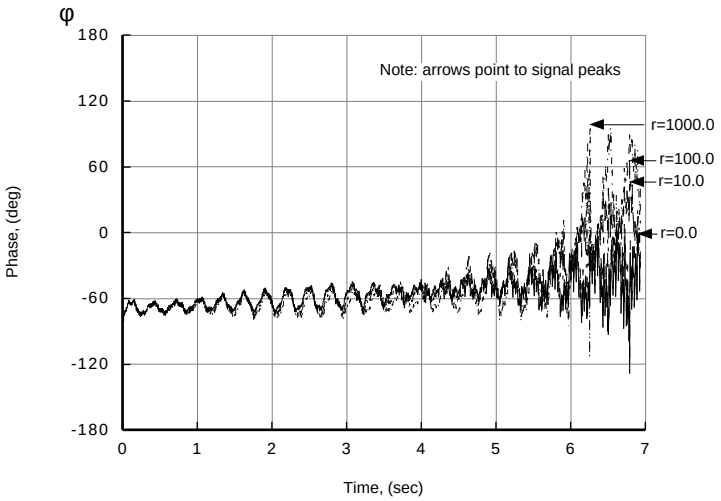

Figure 17: Phase of 4/rev roll accelerations of helicopter for 140 kts ($\mu = 0.330$).

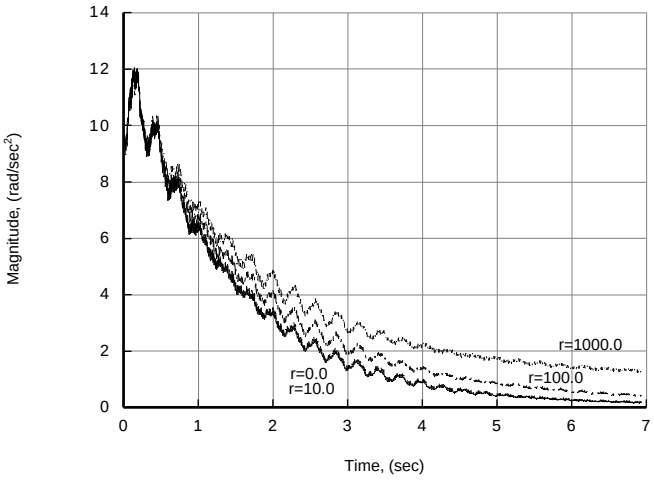

Figure 18: Peak-to-peak 4/rev pitch accelerations of helicopter for 140 kts ($\mu = 0.330$).

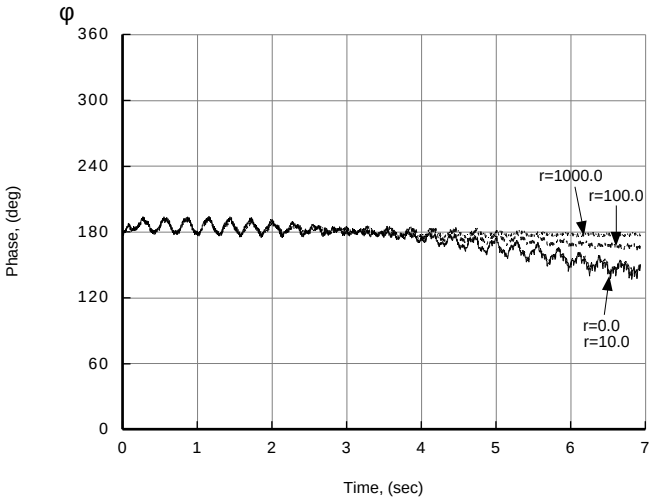

Figure 19: Phase of 4/rev pitch accelerations of helicopter for 140 kts ($\mu = 0.330$).

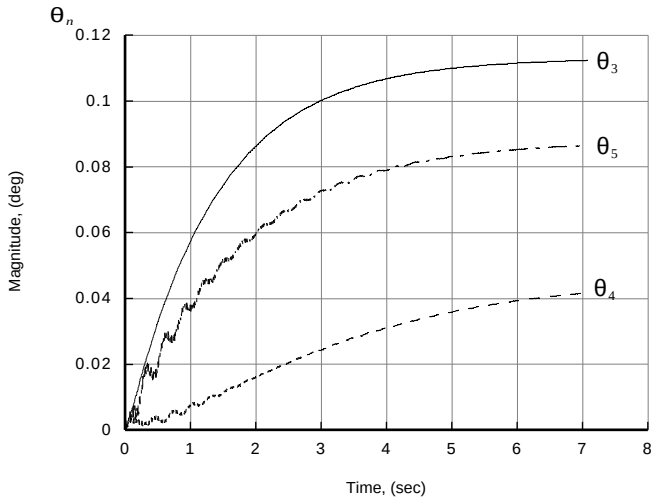

Figure 20: IBC/HHC control input amplitude in degrees, 140 kts ($\mu \approx 0.33$) and r=0.0.

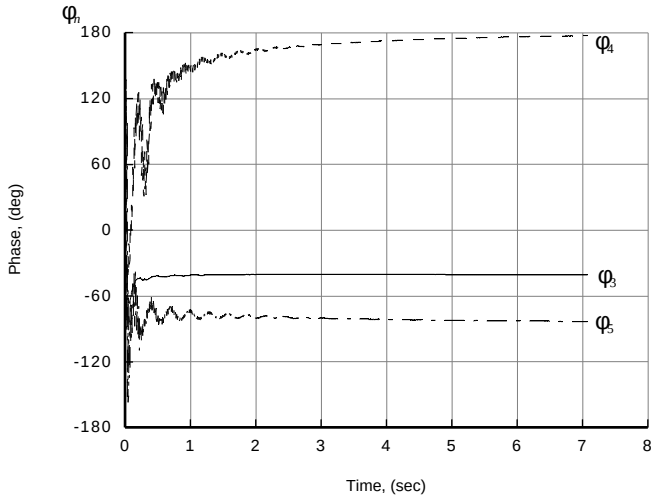

Figure 21: IBC/HHC control input phase in degrees, 140 kts ($\mu \approx 0.33$) and r=0.0.

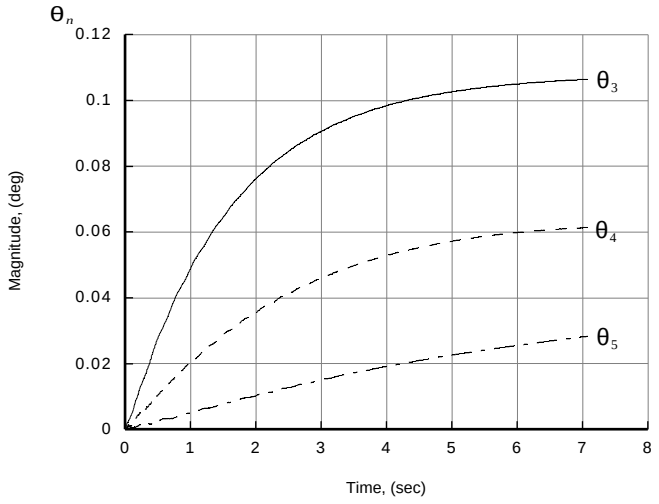

Figure 22: IBC/HHC control input amplitude in degrees, 140 kts ($\mu \approx 0.33$) and r=1000.0.

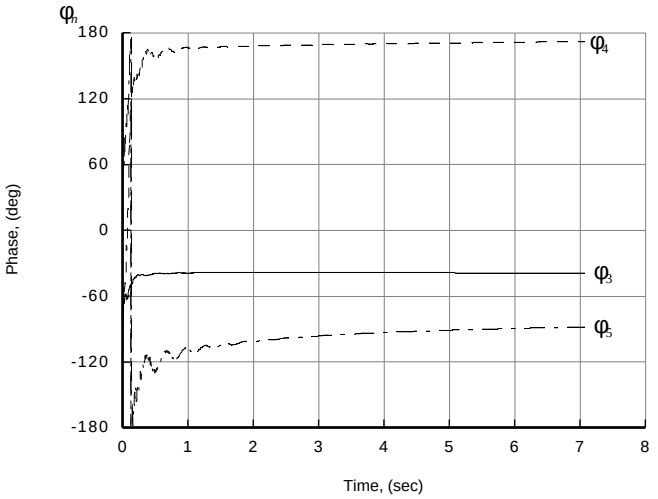

Figure 23: IBC/HHC control input phase in degrees, 140 kts ($\mu \approx 0.33$) and r=1000.0.

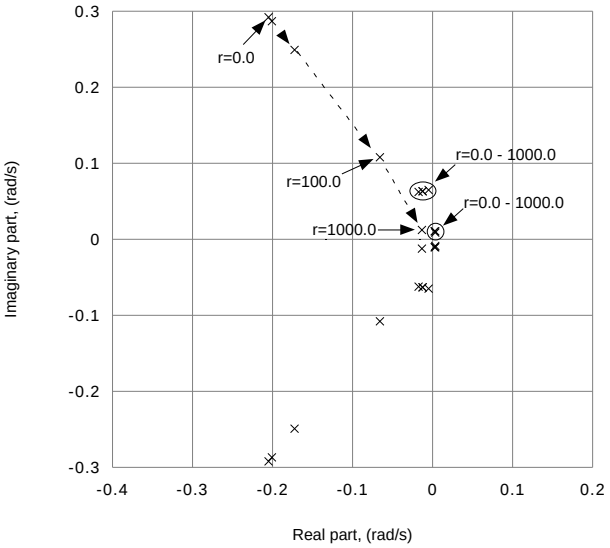

Figure 24: Root-locus of LTI closed-loop system controller poles, 140 kts.

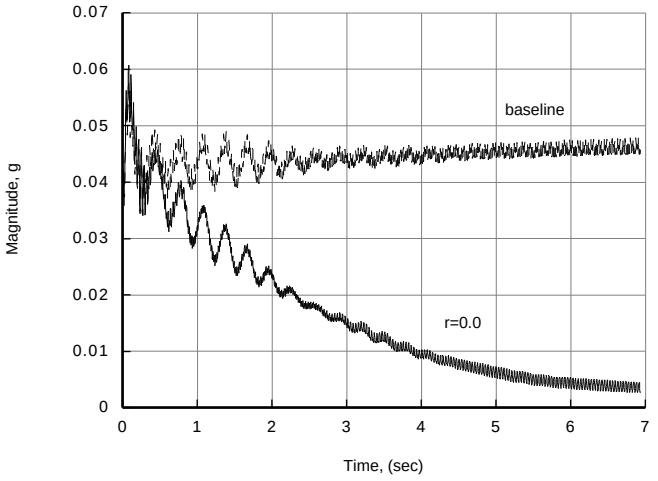

Figure 25: Peak-to-peak 4/rev vertical accelerations of helicopter for 170 kts ($\mu = 0.4$).